The Role of Integrated Approach in the Determination of Nanoparticle Sizes in Dispersions

E. V. Kuznetsova[a, *], **N. M. Kuznetsov**[a], **K. T. Kalinin**[a], **P. V. Lebedev-Stepanov**[b, c],
A. A. Novikov[d], **and S. N. Chvalun**[a, e]

[a] *National Research Center "Kurchatov Institute," Moscow, 123182 Russia*

[b] *Federal Research Center "Crystallography and Photonics," Russian Academy of Sciences, Moscow, 119333 Russia*

[c] *National Research Nuclear University, MEPhI, Moscow, 115409 Russia*

[d] *National University of Oil and Gas "Gubkin University," Moscow, 119991 Russia*

[e] *Enikolopov Institute of Synthetic Polymeric Materials, Russian Academy of Sciences, Moscow, 117393 Russia*

*e-mail: kuznetsova.kate992@gmail.com

Received July 13, 2022; revised August 25, 2022; accepted August 28, 2022

Abstract—Aqueous dispersions of gold and silver nanoparticles (NPs) stabilized with sodium citrate, as well as polymeric NPs based on poly(lactide-*co*-glycolide) (70 : 30 mol %) stabilized with poly(vinyl alcohol) have been obtained. The sizes of NPs have been determined by transmission electron microscopy (TEM), dynamic light scattering (DLS), and analytical ultracentrifugation (AUC). It has been shown that the diameter of both metallic and polymeric particles measured by TEM is significantly lower than their hydrodynamic diameter D_h determined by DLS. Moreover, it has been found that the D_h value obtained for the studied particles from DLS distributions is overestimated compared to that determined by AUC, because the AUC method is less sensitive to the particle size polydispersity and the presence of large objects in a dispersion.

INTRODUCTION

Nowadays, nanoparticles (NPs) are actively used in various fields of industry as dyes, food and cosmetic additives, chemical and biological sensors, catalysts, etc. [1–3]. Moreover, NPs are applied in biomedicine as diagnostic agents [4], agents for photodynamic therapy of cancerous tumors [5], targeted drug delivery systems [6–8], etc.

NPs have unique properties, which significantly depend on their size, shape, surface charge, etc. It is known that size of particles affects their biocompatibility, biodistribution, and ability to penetrate through cellular membranes. For example, in ref. [9], the authors have revealed that intraperitoneal injection of small and large gold NPs (GNPs) with average diameter D smaller than 5 and larger than 50 nm, respectively, has no adverse effect on the health of laboratory mice, while the introduction of GNPs with D values of 8–37 nm leads to the death of most animals within three weeks. Sahin et al. have shown that, at equal weight concentration of polymeric NPs based on a random copolymer poly(lactide-*co*-glycolide) (PLGA), stabilized with poly(vinyl alcohol) (PVA), particles with hydrodynamic diameter D_h of 160 nm more efficiently penetrate into HEK293 cells compared to larger particles with $D_h = 230$ nm [10]. Thus, the accurate determination of NPs sizes is a crucial

task from the viewpoint of their application in biomedicine and the prediction of their effects on organisms.

Currently, the most common and relatively simple methods employed for determining NPs size are transmission electron microscopy (TEM) and dynamic light scattering (DLS). In the TEM method, a thin layer of a sample that was preliminarily dried on a grid is studied using a beam of high-energy electrons (80–300 keV) passing through the sample and interacting with it [11]. The contrast, which arises upon TEM examinations due to the absorption of electrons by a sample, makes it possible to obtain high-resolution images, the analysis of which provides information on the shape and size of studied particles. To obtain reliable and reproducible TEM data, it is necessary to have an adequate number of representative images with a uniform distribution of particles. The number of particles in a sample that can be visualized by TEM, the so-called detection limit, depends on many factors, such as sample preparation, sample volume, and particle size and composition. For example, at the same concentration of silver NPs (SNPs) (0.01 wt/vol %), in a 1-μm^3 sample that contains SNPs with $D = 10$ nm, 18 particles could be visualized, while, in a 55-μm^3 sample containing SNPs with $D = 100$ nm, - ... only one [11]. Among the disadvantages

of the method is the need to remove a solvent at the stage of sample preparation, which may lead to undesirable particles aggregation. Moreover, the analysis of images, which is performed manually or automatically (pixel-by-pixel) using a special software, may lead to inaccuracies and errors in particles size determination. This is because of specific to TEM images noise, which makes it difficult to distinctly determine particle boundaries.

To a greater extent, the preliminary drying of a sample hinders the TEM study of biological objects, because the removal of a solvent may lead to a significant change in their structure. Undesirable structural changes and/or particle aggregation can be prevented by using cryogenic transmission electron microscopy (cryo-TEM), according to which samples are preliminarily frozen rather than dried. Cryo-TEM is successfully employed to study not only biological objects, but also metallic NPs [12, 13], detonation nanodiamonds [14], etc. However, the detection limit, the complexity of selecting freezing conditions, and subsequent processing of images, as well as the high cost of equipment, limit the widespread use of cryo-TEM.

It should be noted that TEM studies of polymeric NPs encounter a number of additional difficulties. Firstly, ultrahigh vacuum and high-intensity ionizing radiation in an electron microscope chamber can lead to heating, contamination with hydrocarbons, and radiolysis of polymers [15]. Secondly, polymeric NPs of the "core−corona" and "Janus" types can be studied by TEM only with the use of the selective contrasting procedure [15]. For example, to employ TEM for studying polymeric "core−corona" NPs, which are formed from amphiphilic block copolymers, such as poly(lactide)-*block*-poly(ethylene oxide) (PLA-*b*-PEO) [16, 17], as well as hydrophobic PLGA copolymers in the presence of PVA as a hydrophilic stabilizer [18, 19], toxic uranyl acetate is commonly used as a negative contrasting agent. In addition, when samples are dried at the stage of sample preparation, the stabilizing corona of particles collapses, and the D value determined for NPs by the TEM method turns out to be significantly lower than the value of their D_h. For example, in [19], the D_h value of PLGA particles (lactide-to-glycolide unit ratio is 75 : 25 mol %; weight-average molecular weight is 19 kDa; polydispersity index is 2.2) stabilized with PVA exceeded the value of D by ~50 nm. Thus, to determine the sizes of both metallic and polymeric NPs and, accordingly, to predict their behavior in a human body, it is necessary to use additional research methods.

In contrast to TEM, DLS allows one to study colloidal solutions of NPs in situ. Moreover, in the DLS method, the obtained experimental data are averaged over a significantly larger number of particles than in the TEM method. DLS measures the time dependence of scattered light intensity fluctuations that result from the Brownian motion of particles in a solu-

tion [20, 21]. The obtained experimental data are represented by the $g_2(\tau)$ autocorrelation function of photocurrent. This function is used to calculate the size distributions of the studied particles, as a rule, with the help of a special software package, such as the "Zetasizer" software [22]. The DLS method, which is widely used to determine the sizes of colloidal NPs, has a number of limitations and disadvantages. For example, when studying the DLS of polydisperse samples, the presence of large particles can hinder the detection of small particles [16, 23, 24], because light scattering intensity I is known to be a power function of the particle diameter ($I \sim D^6$ for particles with $D <$ 100 nm and $I \sim D^2$ for particles with $D > 200$ nm) [25]. The authors in ref. [23] have found that, in the presence of even 5 wt % of large SNPs with $D_h = 55$ or 80 nm, the signal from the main fraction of small SNPs ($D_h = 10$ nm) is absent in the scattered light intensity distribution over D_h values of the particles. In addition, DLS is most often used to characterize spherical particles. The study of nonspherical objects (ellipsoidal particles, rods, disks, lamellas, etc.) is difficult, because the classical DLS method does not take into account the contribution of the rotational motion of particles, and may lead to artifacts, e.g., the appearance of a false peak in the scattered light intensity distribution over D_h values of particles [26].

In addition to TEM and DLS, atomic force microscopy, analysis of particle trajectories, X-ray scattering, analytical ultracentrifugation (AUC), fluorescence correlation spectroscopy, etc., are used to determine the size of colloidal NPs and estimate their polydispersity over sizes [27]. The AUC method is used to study the sedimentation of NPs under the action of the centrifugal force, while the concentration gradients that arise in a sample under centrifugation are detected in real time using an optical system. Experimental data are recorded as concentration profiles $c(r, t)$ depending on radial distance r from the rotor and time t. These profiles can be converted into distributions of sedimentation coefficients $c(s)$ and diffusion coefficients $c(D_f)$ using the "Sedfit" software [28]. In contrast to the DLS method, AUC is more suitable for studying polydisperse systems [29]. Moreover, this method enables one to study the surface of particles [30], interactions of metallic particles with proteins [31], etc. The disadvantages of the method include the complexity of data interpretation, the high cost of equipment, and the long time of the analysis.

In this work, two types of NPs were chosen as the objects of the study: metallic particles (GNPs and SNPs) stabilized with sodium citrate and polymeric (PLGA) particles stabilized with PVA. Using complementary experimental methods, i.e., TEM, DLS, and AUC, the average size and polydispersity of colloidal NPs over sizes were determined. It was shown that the D value of both metallic and polymeric particles increases in a series $D_{TEM} < D_{AUC} < D_{DLS}$ due to the

features of the investigation methods, which are discussed in this article.

EXPERIMENTAL

Materials

Sodium citrate, chloroauric acid ($HAuCl_4$), tannic acid, and silver nitrate ($AgNO_3$) (all produced by Sigma Aldrich, United States) were used as received. Poly(lactide-co-glycolide) (PLGA) was synthesized by ring-opening polymerization. Copolymerization of D,L-lactide (3.92 g) and glycolide (0.98 g) was carried out in melt in a conical flask at 160°C in the presence of ethylene glycol (4.9 mg) as an activator (Sigma Aldrich, United States) and tin octoate (2.45 mg) as a catalyst (Sigma Aldrich, United States) for 3 hours. The reaction product was dissolved in tetrahydrofuran and precipitated with cooled hexane. The ^1H NMR study showed that the ratio of lactide and glycolide units in the copolymer was 70 : 30 mol %. Weight-average molecular mass M_w (97 kDa) and polydispersity index (2.12) of the copolymer were determined by gel-permeation chromatography. PVA (M_w = 30–70 kDa, hydrolyzation degree of 87%) (Sigma Aldrich, United States) was used as received. The organic solvents (special purity grade, Khimreaktiv, Russia) were used as received. Solutions were prepared in deionized water (17.5 MΩ cm) obtained with a Vodolei-M setup (Khimelektronika, Russia).

Preparation of Gold Nanoparticles (GNPs)

GNPs stabilized with sodium citrate were obtained using the modified method proposed by Bastús et al. [32, 33]: twice distilled water (6 mL), a 25 mM $HAuCl_4$ solution (71 μL) and a 60 mM sodium citrate solution (88 μL) were mixed in a 10-mL polypropylene test tube. The resulting solution was incubated in the closed test tube at 90°C for 15 min in a circulating water bath. As a result, a pink-colored GNPs dispersion was obtained, which was then cooled to 15°C in a water bath. The resulting dispersion was stored at 4°C.

Preparation of Silver Nanoparticles (SNPs)

SNPs stabilized with tannin and sodium citrate were obtained using the procedure described by Bastús et al. in ref. [34]: an aqueous solution (100 mL) containing sodium citrate (5 mM) and tannic acid (25 μM) was prepared. Then the solution was placed into a three-necked round-bottom flask and heated to the boiling point of the solvent (100°C) for 15 min under intense stirring. A reflux condenser was used to prevent the solvent from evaporation. After the onset of boiling, a 25 mM $AgNO_3$ solution (1 mL) was added to the reaction mixture, and the solution color became bright yellow. The resulting dispersion was stored at 4°C.

Preparation of Polymeric Nanoparticles

A standard nanoprecipitation procedure [35] was used to obtain PLGA particles stabilized with PVA. A weighed portion (100 mg) of the polymer was dissolved in acetone (10 mL). The obtained solution was added dropwise in to a 5 mg/mL aqueous solution (10 mL) of PVA used as a stabilizer. Acetone was evaporated for 4 hours at room temperature under continuous stirring (700 rpm). The resulting aqueous dispersion was centrifuged (40 000g, 30 min) to remove residual acetone and free PVA. The supernatant was collected, and precipitated PLGA NPs were redispersed in deionized water. The procedure was repeated three times. The resulting dispersion was stored at 4°C.

Dynamic Light Scattering (DLS)

Aqueous dispersions of metallic and polymeric NPs were studied with a Zetasizer Nano ZS analyzer (Malvern Instruments Ltd, United States) equipped with a He−Ne laser operating at a wavelength of 633 nm. The photodetector of the analyzer was located at an angle of 173°. Dispersions with a volume of 1 mL were placed into a quartz cuvette with the optical length of 10 mm, and the measurements were carried out at 25°C. Distributions of the hydrodynamic diameters (D_h) of the NPs in the dispersions were calculated from the autocorrelation functions of the scattered light intensity using the "Zetasizer" software.

Transmission Electron Microscopy (TEM)

Metallic NPs were studied using a JEOL JEM-2100 electron microscope (JEOL Ltd., Japan), which was equipped with an Ultrascan 4000 camera (Gatan, United States) used as a detector and operated at an accelerating voltage of 200 kV in the light field mode. Carbon-coated copper grids were used as substrates. An aqueous dispersion (3 μL) of NPs was applied onto the substrate and incubated for 1 min. Then, the substrate was washed with deionized water (10 μL), and the excess of the solution was removed by contacting the grid edge with a filter paper. Before TEM measurements, the sample was dried for 30 min.

Polymeric NPs were studied using a Titan 80-300 TEM/STEM electron microscope (FEI, United States), which was equipped with a BM-Ultrascan camera (Gatan, United States) and operated at an accelerating voltage of 300 kV in the light field mode. The contrast was enhanced employing the procedure of negative contrasting with uranyl acetate used as a contrasting agent. Carbon-coated copper grids were also used as substrates. An aqueous dispersion (3 μL) of NPs was applied onto the substrate and incubated for 1 min. Then the substrate was washed with deionized water (10 μL), and a 0.5 wt % uranyl acetate solution (10 μL) was immediately applied, and the sample

was incubated for 30 sec. After each step, the excess of the solution was removed by contacting the grid edge with a filter paper. Before the TEM study, the sample was dried for 30 min.

Analytical Ultracentrifugation (AUC)

The high-speed sedimentation of metallic NPs was studied with an Optima AUC analytical ultracentrifuge (Beckman Coulter, United States) using an optical absorption scanning system operating in the UV-Vis spectral region. An "An-60 Ti" four-cell titanium rotor loaded with an analytical cell with a two-sector Epon central element (the optical length of 12 mm) and a balancing cell was placed into the ultracentrifuge. A solution (420 µL) of metallic NPs and a pure citrate buffer ($[\eta_0]$ = 0.001 Pa s, ρ_0 = 0.9971 g/cm^3) (440 µL) used as a solvent were placed into the cell. The rotor rotation speed was 3000 rpm, the absorption was scanned at wavelengths λ = 430 and 525 nm for SNPs and GNPs, respectively. The measurements were carried out at 25°C.

The high-speed sedimentation of polymeric NPs was studied with an Optima AUC analytical ultracentrifuge (Beckman Coulter, United States) using an optical interference system (wavelength λ = 660 nm). "An An-60 Ti" four-cell titanium rotor loaded with an analytical cell with a two-sector Epon central element (the optical length of 12 mm) and a balancing cell was placed into the ultracentrifuge. A solution (420 µL) of polymeric NPs and pure deionized water ($[\eta_0]$ = 0.001 Pa s, ρ_0 = 0.9971 g/cm^3) (440 µL) used as a solvent were placed into the cell. The rotor speed was 5000 rpm. The measurements were carried out at 25°C.

The obtained sedimentation profiles were analyzed using the *Is*−*g***(s)* model with the Tikhonov−Phillips regularization included into the "Sedfit" software [36]. The *Is*−*g***(s)* model describes the sedimentation of nondiffusing particles, and implements the analysis of boundary values by the method of the least squares.

Prior to all measurements, aqueous dispersions of NPs were removed from a refrigerator (4°C) and thermostated at room temperature for 1 h; then, they were sonicated for 15 min.

RESULTS AND DISCUSSION

The safe and efficient use of both metallic and polymeric NPs in biomedicine requires an accurate determination of their size, as well as the assessment of their polydispersity over sizes, because the size of NPs is known to significantly affect their biocompatibility, biodistribution, cell penetration efficiency, etc.

Metallic and polymeric particles were characterized using TEM, DLS, and AUC. Representative TEM images of GNPs and SNPs stabilized with sodium citrate and PLGA particles stabilized with PVA are exhibited in Figs. 1a, 1d, and 1g, respectively.

Metallic particles have predominantly a spherical morphology; however, the obtained images also show GNPs and SNPs of nonspherical shape (indicated by arrows in Figs. 1a and 1d). As one can see in Figs. 1b and 1e, the TEM particle size distributions are mono-modal with a well-defined maximum, the position of which corresponds to the most probable diameter D of GNPs and SLPs, which are equal to 14 and 13 nm, respectively. Average relative half-width of the TEM distribution, $\sigma_{TEM} = \left(\dfrac{\sigma_D}{D} \right) \times 100\%$, where σ_D is the half-width of the distribution at the half-height of a maximum, is equal to 14 and 29% for GNPs and SNPs, respectively. In addition, the analysis of the TEM images yielded the distributions of the aspect ratio D_{max}/D_{min} of metallic particles, i.e. the ratio of maximum particle diameter D_{max} to its minimum diameter D_{min} (Figs. 1c, 1f). The values of D_{max}/D_{min} for GNPs and SNPs vary within ranges of 1.0−1.8 and 1.0−1.4, respectively, while the most probable values of D_{max}/D_{min} are 1.1 ± 0.1 and 1.2 ± 0.1, respectively.

As one can see in from Fig. 1g, PLGA-based polymeric particles also have a spherical morphology. It should be noted that, in an aqueous dispersion, the studied polymeric NPs are represented by hydrophobic PLGA core coated with stabilizing PVA corona, which prevents the aggregation of particles and their separation into a separate phase (precipitate) [18, 19]. Upon the immobilization of the sample onto the substrate and its subsequent drying, the stabilizing PVA layer collapses [18, 19]. Thus, the TEM method makes it possible to estimate only the diameter of PLGA core (indicated by the arrow in Fig. 1g), which is significantly smaller than the average particle diameter in the solvated state. The obtained TEM distribution is monomodal with a well-defined maximum (Fig. 1h), the position of which corresponds to the value of D equal to 52 nm (σ_{TEM} = 30%).

Aqueous dispersions of metallic and polymeric NPs were studied by DLS. A bimodal scattered light intensity distribution over hydrodynamic diameters D_h of the particles was found for GNPs (Fig. 2a). The positions of the maxima of the major and minor peaks on the DLS distribution correspond to the D_h values equal to 35 and 2 nm, respectively. In this case, the automatic recalculation of the scattered light intensity distribution using the Zetasizer software into the particle volume and number size distributions yielded monomodal distributions with maxima at ~2 nm (Fig. 2b). It should be noted that, when analyzing the TEM images, no GNPs with D smaller than 5 nm were detected (Fig. 1b).

Previously, Khlebtsov et al. performed a DLS study of an aqueous dispersion of GNPs with an average diameter of 60 nm and also found a bimodal distribu-
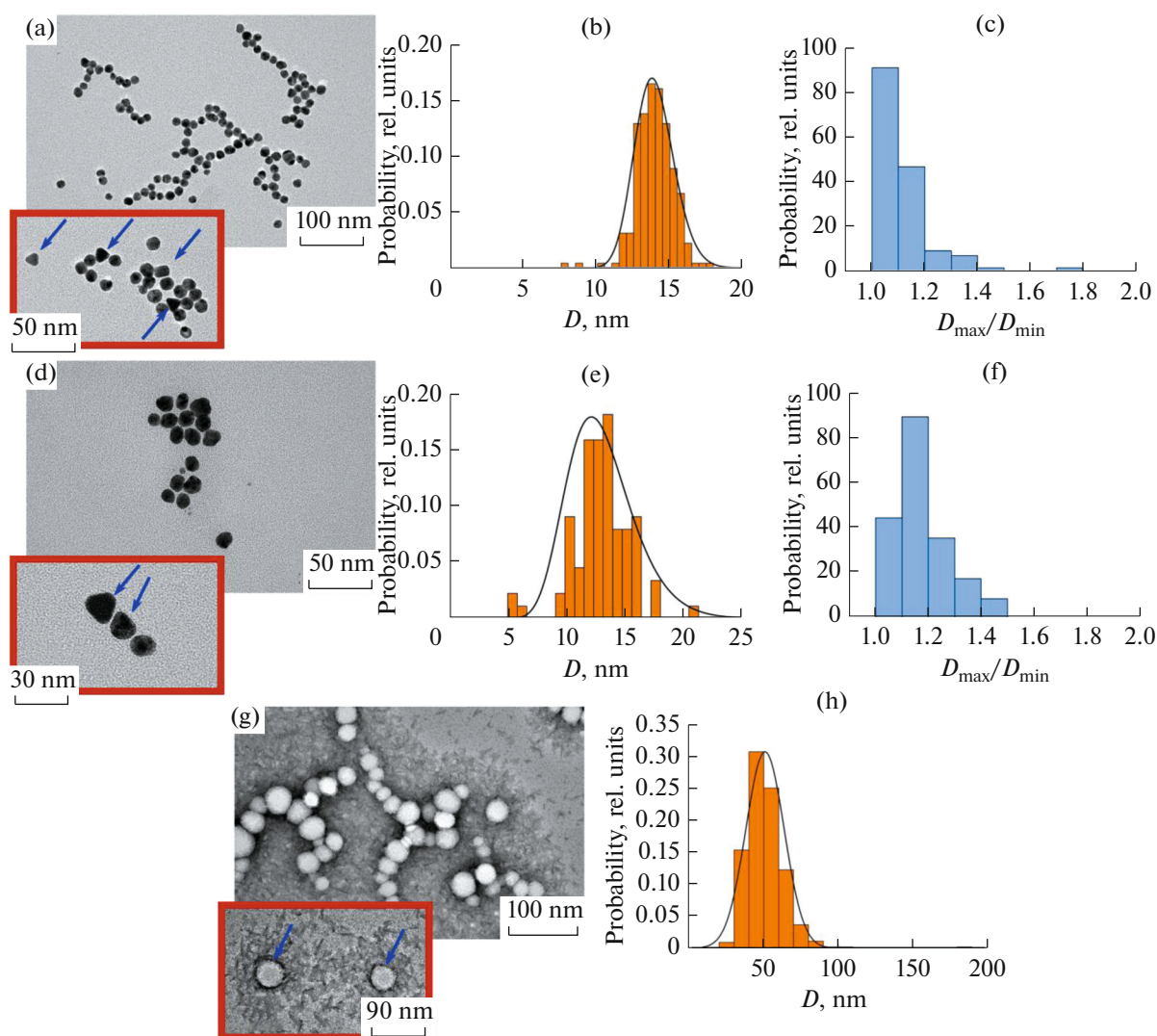
Fig. 1. Representative TEM images of (a) GNPs, (d) SNPs, and (g) PLGA NPs. Diameter (D, nm) distribution histograms of the (b) GNPs, (e) SNPs and (h) PLGA NPs evaluated from the TEM images. Aspect ratio (D_{max}/D_{min}) distribution histograms of the (c) GNPs and (f) SNPs evaluated from the TEM images. The arrows in Fig. 1a and 1d show nonspherical metallic NPs. The arrows in Fig. 1h denote PLGA cores surrounded by PVA coronas.

tion of scattered light intensity over D_h values of the particles with major (~59 nm) and minor (~5−6 nm) maxima [37]. The authors revealed that the appearance of the false minor peak of small sizes in the DLS distribution is associated with the contribution of rotational diffusion to the measured correlation function due to the anisotropy of the studied GNPs (according to TEM data, the value of aspect ratio of the particles was 1.33 ± 0.22). We suppose that, the bimodal scattered light intensity distribution observed for the studied in this work GNPs (Fig. 2a) can be related to the presence of a certain number of anisotropic GNPs with $D_{max}/D_{min} > 1.1$ in the dispersion (Fig. 1c).

It should be noted that the D_h value of GNPs corresponding to the position of the major maximum in the DLS intensity distribution (Fig. 2a) is larger

2.5 fold than the value of D evaluated from the TEM images (Table 1). Therefore, the σ_{DLS} value for the major peak of the DLS distribution is larger ~5 fold compared with the relative width of the TEM histogram (Table 1).

For an aqueous dispersion of SNPs, a monomodal distribution of the scattered light intensity over particle D_h has been observed (Fig. 2c). The D_h value corresponding to the maximum on the obtained DLS distribution is 21 nm. The recalculation of the scattered light intensity distribution into the particle volume and number size distributions has yielded monomodal distributions with maxima at 16 and 13 nm, respectively (Fig. 2d). It seems that the mononodality of the DLS distribution of the SNPs is achieved due to narrow aspect ratio distribution of the silver particles
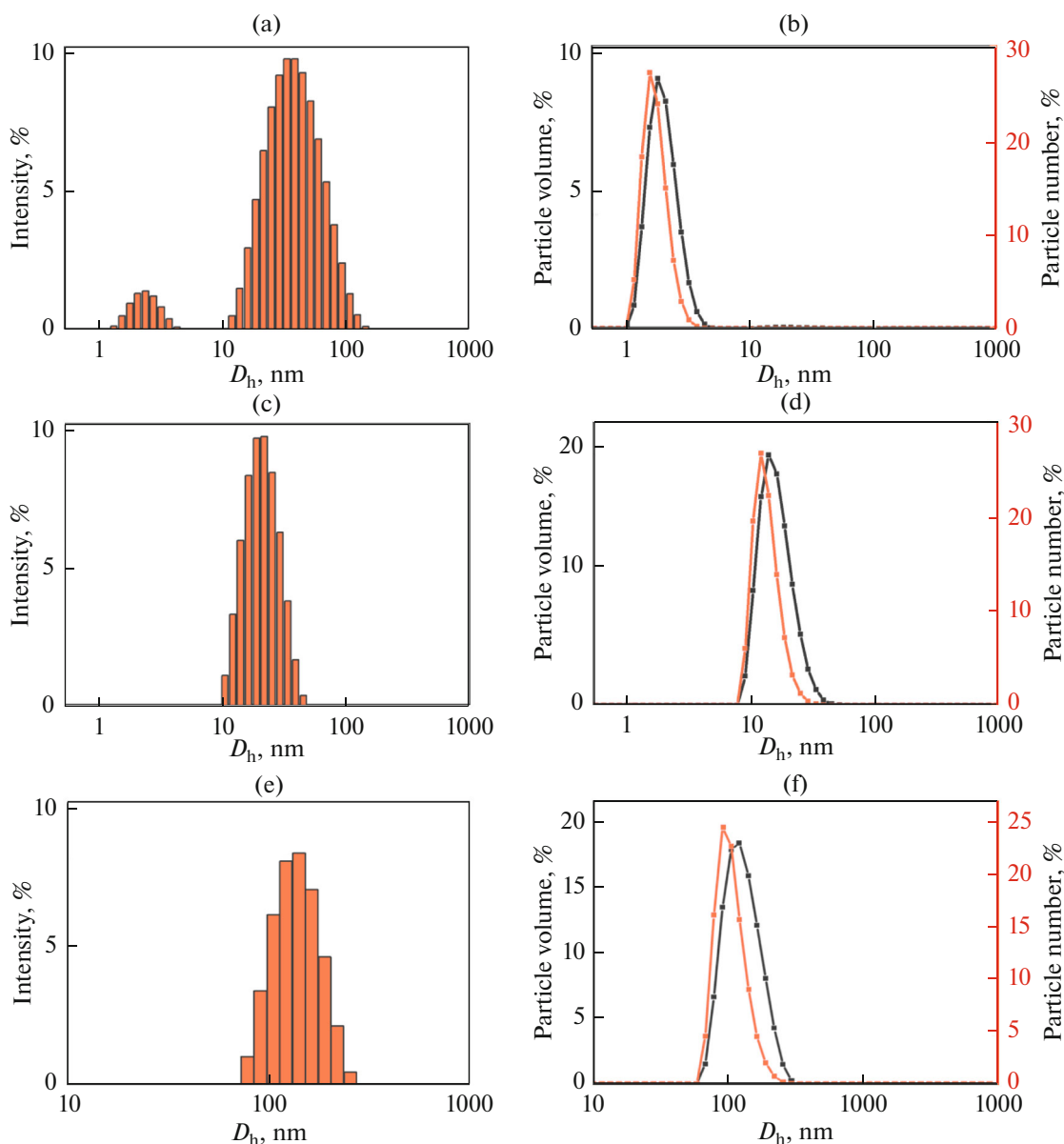
Fig. 2. DLS intensity hydrodynamic diameter (D_h, nm) distribution histograms for aqueous dispersions of the (a) GNPs, (c) SNPs and (e) PLGA NPs. The DLS volume and number D_h distribution curves for aqueous dispersions of the (b) GNPs, (d) SNPs, and (f) PLGA NPs.

compared to that of the GNPs (Figs. 1c, 1f). The relative width of the DLS intensity distribution is larger ~1.4 fold than the relative width of the TEM distribution (Table 1).

For an aqueous dispersion of PLGA particles stabilized with PVA, we have also found a monomodal scattered light intensity distribution over the D_h values of the NPs (Fig. 2e). The value of D_h corresponding to the maximum on the resulting distribution, is 141 nm. The automatic recalculation of the DLS intensity distribution into the particle volume and number size distributions has led to monomodal distributions with maxima at 132 and 108 nm, respectively (Fig. 2f). The

D_h value of PLGA NPs significantly exceeds (~2.7 fold) their D value. This may be due to the fact that, when studying the PLGA particles by the DLS method, the stabilizing hydrophilic PVA corona is in a swollen state because of the solvation with solvent molecules, while, when studying the particles by the TEM method, the PVA corona is, on the contrary, collapsed [18, 19]. Therefore, the relative width of the DLS intensity distribution is ~1.3 fold larger than that of the TEM histogram (Table 1).

As ona can see in Table 1, the D values of the metallic and polymeric NPs have turned out to be lower than the corresponding values of D_h by a factor of

Table 1. Average sizes of metallic and polymeric NPs as well as average relative half-widths of the size distributions evaluated from the TEM, DLS, and AUC

Sample	D, nm (TEM)	σ_{TEM}, %	D_h, nm (DLS)	σ_{DLS}, %	D_h, nm (AUC)	σ_{AUC}, %
Metallic NPs						
GNPs	14	14	35	75	22	14
SNPs	13	29	21	41	16	11
Polymeric NPs						
PLGA	52	30	141	39	111	29

1.75−2.7, while the most significant difference is observed for the PLGA particles. Thus, in contrast to DLS, the TEM method cannot determine the average size of the studied particles in the solvated state. At the same time, it is worth noting that, due to the high sensitivity of the DLS to polydispersity and the presence of large particles in a sample, the values of D_h experimentally determined for NPs may be overestimated [38, 39]. Therefore, AUC was chosen as an additional method for evaluation of the average size of NPs in the solvated state, as well as for estimating the width of the size distribution in this work.

The representative experimental sedimentation profiles, i.e. concentration profiles $c(r, t)$ depending on radial distance from the rotor r and time t, obtained in the absorption and interference modes for aqueous dispersions of GNPs and PLGA particles are shown in Figs. 3a and 3b, respectively.

Distribution of sedimentation coefficients $c(s)$, where s is the ratio of the particle sedimentation rate in a solvent to the applied acceleration, calculated using the "Sedfit" program for GNPs has a well-defined maximum, the position of which corresponds to the value of $s_{max} \sim 3600$ S (Fig. 4a). It was observed that besides the major GNPs fraction with $s_{max} \sim 3600$ S, the dispersion contains particles for which the value of s varies in a rather wide range from 5000 to 13 000 S. The $c(D_h)$ distribution obtained by the automatic recalculation of the $c(s)$ distribution using the "Sedfit" software is shown in Fig. 4b. The D_h value corresponding to the position of the maximum in $c(D_h)$, is 22 nm, the average relative half-width of the σ_{AUC} distribution is equal to 14%. The comparison between the TEM histogram (Fig. 1b), the DLS intensity size distribution (Fig. 2a), and the $c(D_h)$ distribution (Fig. 4b) for GNPs has indicated that the minor peak observed in the DLS distribution within a size range of ~2−5 nm is false, because no particles of such a small size have been found by the TEM and AUC methods. In addition, when a dispersion of GNPs was centrifuged at higher speed (10000 rpm), small particles ($D_h <$ 10 nm) did not sediment.

The AUC method was also employed to study the aqueous dispersion of SNPs. The $c(s)$ and $c(D_h)$ distributions calculated for the particles are shown in Figs. 4c and 4d, respectively. According to the calculated $c(s)$ distribution, the main fraction in the dispersion consists of SNPs with $s_{max} \sim 800$ S; however, a small fraction of particles with $s \sim 290$ S and particles for which s varies within a range of 1200−4000 S is also presented (Fig. 4c). The $c(D_h)$ distribution of silver particles has a well-defined maximum corresponding to the D_h value of 16 nm. We observed that, as compared with GNPs (Fig. 4b), the fraction of large SNPs with $s > s_{max}$ has turned out to be lower (Fig. 4d).

The $c(s)$ and $c(D_h)$ distributions calculated for PLGA particles stabilized with PVA are shown in Figs. 4e and 4f, respectively. According to the obtained $c(s)$ distribution, the main fraction in the dispersion consists of particles with $s_{max} \sim 430$ S; however, particles, for which s varies in a range of 1000−5000 S are also presented (Fig. 4e). The $c(D_h)$ distribution of particles is characterized by a distinct maximum corresponding to the D_h value of 111 nm. It should be noted that previously, in [19], an aqueous dispersion of PVA-stabilized particles of PLGA with a similar molecular composition (75 : 25 mol %) was studied by small-angle X-ray scattering (SAXS). According to the SAXS data, the size of the scattering object D_{max}, which takes into account the contribution of the PLGA core and PVA corona, is 100 nm. Thus, the value of D_h obtained by DLS appears to be overestimated in comparison with the PLGA particle size determined by the AUC and SAXS methods.

CONCLUSIONS

Aqueous dispersions of metallic and polymeric NPs have been studied by TEM, DLS, and AUC. It has been shown that, depending on the method of determination, particle diameter D increases in a series $D_{TEM} < D_{AUC} < D_{DLS}$. The smaller values of D_{TEM}, as compared with D_{AUC} and D_{DLS} are associated with the particularity of the sample preparation. Thus, the immobilization of a dispersion on a substrate fol-
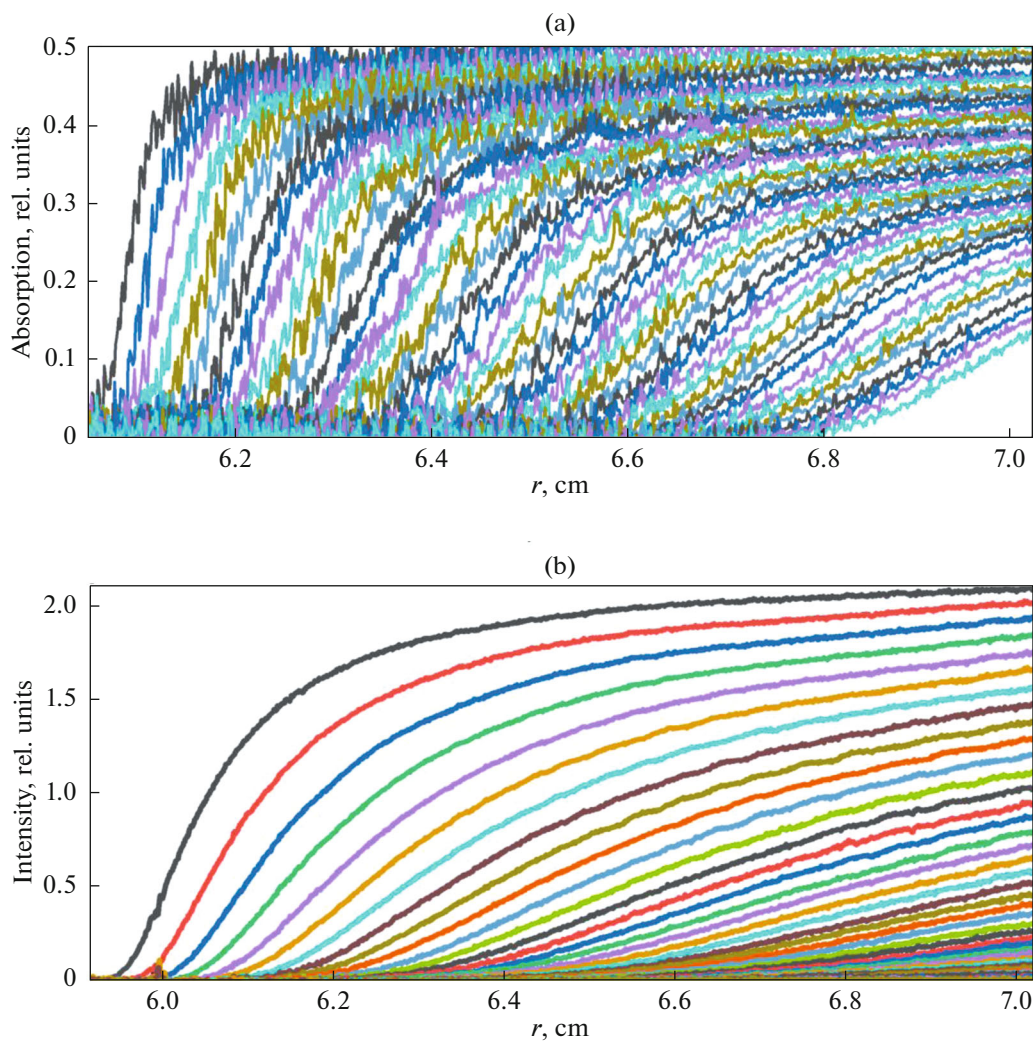
Fig. 3. Experimental sedimentation profiles obtained for aqueous dispersions of the (a) GNPs and (b) PLGA NPs in the absorption and interference modes, respectively.

lowed by its drying results in the desolvation of the hydrophilic stabilizer molecules adsorbed on the surface of the particles core and, correspondingly, to the collapse of the stabilizing corona. Hence, the TEM method enables one to visualize the shape and estimate the size and polydispersity of the core sizes of metallic and polymeric NPs; however, it does not provide information on the size of solvated particles, which is necessary for their safe and efficient application in biomedicine. On the contrary, the DLS method is suitable for determining the NPs size directly in a solution; however, the D_{DLS} values of the particles are overestimated compared with the D_{AUCs} values, because, in the case of the DLS, the polydispersity of NPs sizes and the presence of even small amount of large particles affect the accuracy of size determination to a greater extent.

Thus, the characterization of various types of the NPs (determination of their size and shape) requires the application of several complementary experimental methods. The use of TEM as a basic method does not provide the complete information on the size of particles in a dispersion because of its locality and the impossibility of taking into account the contribution of the solvate corona to the particle size. Therefore, additional studies should always be carried out with at least one integral method.
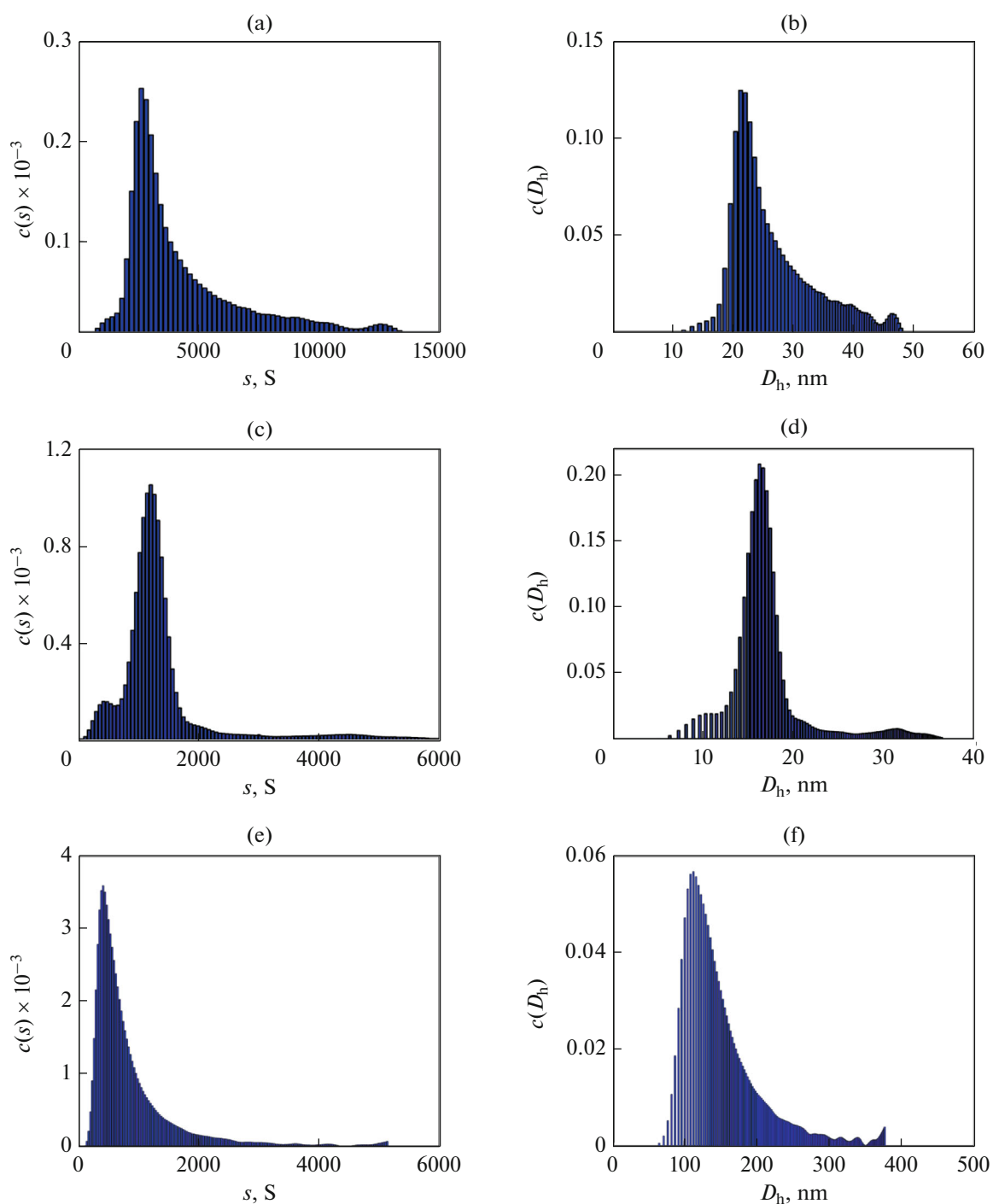
Fig. 4. The sedimentation coefficient (s, S) distribution histograms for aqueous dispersions of the (a) GNPs, (c) SNPs, and (e) PLGA NPs and the corresponding hydrodynamic diameter (D_h, nm) distribution histograms of the (b) GNPs, (d) SNPs, and (f) PLGA NPs calculated from the AUC.

CONFLICT OF INTEREST

The authors declare that they have no conflicts of interest.

SUPPLEMENTARY INFORMATION

The online version contains supplementary material available at https://doi.org10.1134/S1061933X22600348.

REFERENCES

1. Stark, W.J., Stoessel, P.R., Wohlleben, W., and Hafner, A., *Chem. Soc. Rev.,* 2015, vol. 44, p. 5793. https://doi.org/10.1039/C4CS00362D

2. Aithal, S., Mishriki, S., Gupta, R., et al., *Talanta,* 2022, vol. 236, p. 122841. https://doi.org/10.1016/j.talanta.2021.122841

3. Nguyen, T.H.A., Nguyen, V.C., Phan, T.N.H., et al., *Chemosphere,* 2022, vol. 287, no. 3, p. 132271. https://doi.org/10.1016/j.chemosphere.2021.132271

4. Salavatov, N.A., Bol'shakova, A.V., Morozov, V.N., et al., *Colloid J.,* 2022, vol. 84, p. 93. . https://doi.org/10.1134/S1061933X22010100

5. Bucharskaya, A.B., Khlebtsov, N.G., Khlebtsov, B.N., et al., *Materials,* 2022, vol. 15, no. 4, p. 1606. https://doi.org/10.3390/ma15041606

6. Xiang, Q., Wu, Z., Tian, E.-K., et al., *J. Biomater. Tissue Eng.,* 2022, vol. 12, no. 3, p. 445. https://doi.org/10.1166/jbt.2022.2934

7. Miranda, R.R., Sampaio, I., and Zucolotto, V., *Colloids Surf., B,* 2022, vol. 210, p. 112254. https://doi.org/10.1016/j.colsurfb.2021.112254

8. Sedush, N.G., Kadina, Y.A., Razuvaeva, E.V., et al., *Nanobiotechnology Reports,* 2021, vol. 16, no. 4, p. 421. . https://doi.org/10.1134/S2635167621040121

9. Chen, Y.-S., Hung, Y.-C., Liau, I., and Huang, G.S., *Nanoscale Res. Lett.,* 2009, vol. 4, p. 858. https://doi.org/10.1007/s11671-009-9334-6

10. Sahin, A., Esendagli, G., Yerlikaya, F., et al., *Artif. Cells, Nanomed., Biotechnol.,* 2017, vol. 45, no. 8, p. 1657. https://doi.org/10.1080/21691401.2016.1276924

11. Dudkiewicz, A., Tiede, K., Loeschner, K., et al., *Trends Anal. Chem.,* 2011, vol. 30, p. 28. https://doi.org/10.1016/j.trac.2010.10.007

12. Kamyshinsky, R.A., Kuznetsov, N.M., Lebedev-Stepanov, P.V., et al., *Crystallogr. Rep.,* 2021, vol. 66, no. 4, p. 612. https://doi.org/10.1134/S106377452104009X

13. Mikhutkin, A.A., Kamyshinsky, R.A., Kuznetsov, N.M., et al., *Nanobiotechnology Reports,* 2022, vol. 17, no. 3, p. 396. . https://doi.org/10.1134/S2635167622030119

14. Kuznetsov, N.M., Belousov, S.I., Bakirov, A.V., et al., *Carbon,* 2020, vol. 161, p. 486. https://doi.org/10.1016/j.carbon.2020.01.054

15. Renz, P., Kokkinopoulou, M., Landfester, K., and Lieberwirth, I., *Macromol. Chem. Phys.,* 2016, vol. 217, p. 1879. https://doi.org/10.1002/macp.201600246

16. Razuvaeva, E.V., Kulebyakina, A.I., and Streltsov, D.R., et al., *Langmuir,* 2018, vol. 34, p. 15470. https://doi.org/10.1021/acs.langmuir.8b03379

17. Kadina, Y.A., Razuvaeva, E.V., Streltsov, D.R., et al., Molecules, 2021, vol. 26, p. 602. https://doi.org/10.3390/molecules26030602

18. Razuvaeva, E.V., Kalinin, K.T., Sedush, N.G., et al., *Mendeleev Commun.,* 2021, vol. 31, p. 512. https://doi.org/10.1016/j.mencom.2021.07.025

19. Razuvaeva, E., Sedush, N., Shirokova, E., et al., *Colloids Surf., A,* 2022, vol. 648, p. 129198.
https://doi.org/10.1016/j.colsurfa.2022.129198

20. Brar, S.K. and Verma, M., *Trends Anal. Chem.,* 2011, vol. 30, no. 1, p. 4.
https://doi.org/10.1016/j.trac.2010.08.008

21. Bhattacharjee, S., *J. Controlled Release,* 2016, vol. 235, p. 337.
https://doi.org/10.1016/j.jconrel.2016.06.017

22. Dynamic Light Scattering (DLS), Malvern, UK. www.malvernpanalytical.com/en/products/technology/light-scattering/dynamic-light-scattering. Accessed July 13, 2022.

23. Tomaszewska, E., Soliwoda, K., Kadziola, K., et al., *J. Nanomater.,* 2013, vol. 2013, p. 60.
https://doi.org/10.1155/2013/313081

24. Desyatskova, A.M., Razuvaeva, E.V., Puchkova, Y.A., et al., *Mendeleev Commun.* (in press).

25. Stetefeld, J., MeKenna, S.A., and Patel, T.R., *Biophys. Rev.,* 2016, vol. 8, p. 409.
https://doi.org/10.1007/s12551-016-0218-6

26. Khlebtsov, B.N. and Khlebtsov, N.G., *Colloid J.,* 2011, vol. 73, no. 1, p. 118.
https://doi.org/10.1134/S1061933X11010078

27. Saprykin, A.I. and Samoilov, P.P., *Ekologiya. Seriya Analiticheskikh Obzorov Mirovoi Literatury,* 2020, no. 109, p. 1.

28. Analytical ultracentrifugation (AUC). Sedfit. https://sedfitsedphat.github.io/sedfit.htm. Accessed July 13, 2022).

29. Carney, R.P., Kim, J.Y., Qian, H., et al., *Nat. Commun.,* 2011, vol. 2, p. 335.
https://doi.org/10.1038/ncomms1338

30. Krpetic, Z., Davidson, A.M., Volk, M., et al., *ACS Nano,* 2013, vol. 7, no. 10, p. 8881.
https://doi.org/10.1021/nn403350v

31. Bekdemir, A. and Stellacci, F., *Nat. Commun.,* 2016, vol. 7, p. 13121.
https://doi.org/0.1038/ncomms13121

32. Bastús, N.G., Comenge, J., and Puntes, V., *Langmuir,* 2011, vol. 27, no. 17, p. 11098.
https://doi.org/10.1021/la201938u

33. Gorbachevskii, M.V., Kopitsyn, D.S., Kotelev, M.S., et al., *RSC Adv.,* 2018, vol. 8, p. 19051.
https://doi.org/10.1039/C8RA00417J

34. Bastús, N.G., Merkoçi, P., Piella, J., and Puntes, V., *Chem. Mater.,* 2014, vol. 26, no. 9, p. 2836.
https://doi.org/10.1021/cm500316k

35. Fessi, H., Puisieux, F., Devissaguet, J.Ph., et al., *Int. J. Pharm.,* 1989, vol. 55, p. 1.
https://doi.org/10.1016/0378-5173(89)90281-0

36. Schuck, P., *Biophys. J.,* 2000, vol. 78, no. 3, p. 1606.
https://doi.org/10.1016/S0006-3495(00)76713-0

37. Khlebtsov, B.N., Khanadeev, V.A., Pylaev, T.E., and Khlebtsov, N.G., *Izv. Sarat. Univ. Nov. Ser. Ser. Fizika,* 2017, vol. 17, no. 2, p. 71.

38. Souza, T.G.F., Ciminelli, V.S.T., and Mohallem, N.D.S., *J. Phys.: Conf. Ser.,* 2016, vol. 733, p. 012039.
https://doi.org/10.1088/1742-6596/733/1/012039

39. Filipe, V., Hawe, A., and Jiskoot, W., *Pharm. Res.,* 2010, vol. 27, p. 796.
https://doi.org/10.1007/s11095-010-0073-2